

# Theoretical investigation of the abnormal Reimer–Tiemann reaction

R. Castillo,<sup>1\*</sup> V. Moliner,<sup>1</sup> J. Andrés,<sup>1</sup> M. Oliva,<sup>1</sup> V. S. Safont<sup>1</sup> and S. Bohm<sup>2</sup>

<sup>1</sup>Departament de Ciències Experimentals, Universitat Jaume I, Box 224, 12080 Castelló, Spain

<sup>2</sup>Department of Organic Chemistry, Institute of Chemical Technology, 16628 Prague 6, Czech Republic

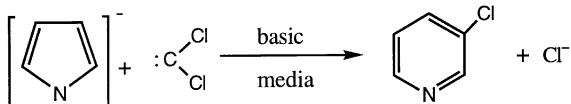
Received 21 July 1997; revised 21 December 1997; accepted 6 January 1998

**ABSTRACT:** The molecular mechanism for the pyrrole ring expansion to yield 3-chloropyridine, as a model of the abnormal Reimer–Tiemann rearrangement, was characterized theoretically *in vacuo* by means of the HF/6–31G\* computational method. The electron correlation was estimated at the MP2/6–31G\* level and by calculations based on density functional theory, B3LYP/6–31G\* and B3LYP/6–31+G\*. Solvent effects of the diethyl ether and ethanol media were analyzed by using a polarizable continuum model. The stationary points were characterized with analytical gradient techniques in the gas phase and insolvents. The topology of the potential energy surfaces calculated at the MP2/6–31G\* and B3LYP/6–31G\* levels shows that the molecular mechanism corresponds to an inverted energy profile along one intermediate, associated with the addition of dichlorocarbene at the  $\beta$ -position of the pyrrole anion, and only one transition structure related to the ring expansion associated with the breaking and forming of  $C\alpha$ – $C\beta$  and  $C$ – $C\alpha$  bonds, respectively, and the  $Cl^-$  leaving process. © 1998 John Wiley & Sons, Ltd.

**KEYWORDS:** abnormal Reimer–Tiemann reaction; theoretical study

## INTRODUCTION

The Reimer–Tiemann rearrangement for the preparation of substituted rings is a useful tool in organic synthesis and an appreciable number of experimental studies on this reaction have been published.<sup>1–7</sup> In particular, the ring expansion of the pyrrole system to form 3-substituted pyridines in the presence of dihalomethanes in a strongly basic medium is an interesting synthetic procedure in organic chemistry.<sup>8–13</sup> This ring enlargement is known as an abnormal Reimer–Tiemann reaction.<sup>11,13</sup> The molecular mechanism reported in the literature clearly establishes that the dichlorocarbene generated *in situ* reacts with the deprotonated pyrrole ring. We chose the reaction of the pyrrole system with dichlorocarbene to yield 3-chloropyridine in strongly basic media as the calculation model:



As a part of a research program devoted to the study of solvent effects on the molecular mechanism of different chemical reactions,<sup>14–16</sup> in the present study we thought it

of interest to undertake *ab initio* calculations, with the aim of gaining further insight into the abnormal Reimer–Tiemann reaction of the pyrrole ring system. To our knowledge, this is the first theoretical study devoted to elucidating the molecular mechanism for this type of ring expansion. We addressed the following problems: (i) the nature of the reaction pathway, which requires a detailed knowledge of stationary points, i.e. reactants, transition structure (TS), products and intermediates, on the potential energy surface (PES); (ii) knowledge of the barrier heights associated with TSs and reaction energies, for which purpose the dependence of the energies and geometries of the stationary structures along the reaction pathway and the transition vectors associated with the transition structures upon theoretical methods were also analyzed; and (iii) the importance of the inclusion of the solvent effects in the characterization of the molecular mechanisms. To clarify the above problems, we carried out full geometry optimization with analytical gradient techniques *in vacuo* and in a solvent at the *ab initio* level of theory, including energy correlation effects.

In the next section, we briefly outline the computational procedures used for the quantum mechanical calculations. In the subsequent section, we describe and discuss the results, analyzing the structure and energy along the reaction path in the gas phase and in a solvent. The analysis of the transition vectors allows us to decide which variables control the transformations. The evolution of the bond breaking/forming processes help us to

\*Correspondence to: R. Castillo, Departament de Ciències Experimentals, Universitat Jaume I, Box 224, 12080 Castelló, Spain.  
Contract/grant sponsor: Ministerio de Educación, DGICYT; contract grant number: PB93-0661.

discuss the results and to explain the nature of the chemical rearrangement.

## COMPUTATIONAL PROCEDURES

*In vacuo* calculations were carried out with the Gaussian 94 package of programs.<sup>17</sup> *Ab initio* calculations were performed at the Hartree–Fock (HF) level. The electron correlation was considered by using the MP2 perturbation theory<sup>18</sup> and methods based on density functional theory (DFT).<sup>19–21</sup> The B3LYP procedure was selected, corresponding to Becke's exchange functional (B),<sup>22,23</sup> which includes a mixture of HF and the Slater exchange along with corrections involving the gradient of the density, and the correlation functional of Lee, Yang and Parr, which includes both local and non-local terms (LYP).<sup>24,25</sup> The standard 6–31G\* basis set was used at all levels of calculation while the inclusion of diffuse functions was considered at the B3LYP/6–31+G\* level.

The PESs were calculated in detail to ensure that all relevant stationary points were located and properly characterized. The exact location of the TS was achieved by using an algorithm<sup>26–28</sup> in which the coordinates describing the system are separated into two sets: the control space, which is responsible for the unique negative eigenvalue in the respective force constants matrix, and the remaining coordinates set that is called complementary space. The geometry optimizations were carried out alternatively on each subspace, one at a time, until a stationary structure was obtained. Finally, a complete analytical optimization of the TS structure was achieved with an ‘eigenvalue following’ optimization method<sup>29,30</sup> for all variables and by means of a normal mode analysis. The intrinsic reaction coordinate (IRC)<sup>31</sup> pathways, from the TSs down to the two lower energy structures, were traced using the second-order González–Schlegel integration method<sup>32,33</sup> in order to verify that each saddle point links the two putative minima.

The required convergence on the density matrix was  $10^{-9}$  atomic units and the threshold value of maximum displacement was 0.0018 Å and that of maximum force was 0.00045 hartree bohr<sup>-1</sup> using the Berny analytical gradient optimization routine.<sup>34,35</sup> The nature of each stationary point was checked by diagonalizing the Hessian matrix to determine the number of imaginary frequencies (zero for the local minima and one for the TSs). The unique imaginary frequency associated with the transition vector (TV)<sup>36</sup> of the different TSs was analyzed.

We included electrostatic solvent interactions in the study of the reaction mechanisms, thereby attempting to identify the influence of the solvent on the nature of the reaction pathway. The effect of solute–solvent interactions was taken into account mostly via the SCRF-PAC package<sup>37</sup> implemented in Gaussian 94.

In the methods based on continuous distributions of the

solvent (for a recent overview, see Ref. 38) this one is assimilated to a continuous medium, characterized by the dielectric constant ( $\epsilon$ ), which surrounds a cavity in which the solute is placed. A dipole in the solute induces a dipole in the medium, and the electric field applied to the solute by the induced solvent dipole (reaction dipole) in turn interacts with the molecular dipole to lead to a net stabilization. The solute–solvent interaction is treated as a perturbation of the Hamiltonian of the isolated molecule.

In this work we employed the continuum model of Rivail and co-workers<sup>39–41</sup> based on the use of cavities, and a multipolar expansion of the solute electrostatic potential. Calculations were made using ellipsoidal cavities surrounded by a continuum of dielectric constant equal to 4.2 for diethyl ether and 24.3 for ethanol and multipolar expansion up to order 6. We reoptimized the stationary points on the PES using the continuum model described above. The first derivatives of the electrostatic term were obtained analytically<sup>41</sup> and the second derivatives were computed numerically. The multipole expansion of the potential converges rapidly but in some cases, namely when the molecular shape is irregular, a multicenter expansion<sup>42</sup> may be necessary to ensure convergence.

## RESULTS AND DISCUSSION

The energy profiles for the process *in vacuo* and in solvent medium are shown in Fig. 1 and 2, respectively, and the relative energies for the stationary points along the reaction pathway are presented in Table 1. The structures associated with the stationary points and the atoms numbering are illustrated in Fig. 3. The calculated structures are named as follows: the reactants (deprotonated pyrrole + dichlorocarbene) are designated **R**, the products (3-chloropyridine + Cl<sup>-</sup>) are termed **P** and the structures corresponding to transition structures and intermediates are designated **TS** and **I**, respectively.

### Gas-phase calculations

The most relevant geometric variables of the stationary points calculated with different methods are reported in Table 2. Optimized geometries of all structures obtained with different computing methods are available from the authors on request. The CCl<sub>2</sub> nucleophilic attack on the  $\beta$ -position of the pyrrole ring takes place in a barrierless fashion, with formation of an intermediate, **I1**, at the HF, MP2 and B3LYP calculation levels, located on a very flat region on the PES, i.e. the lower positive vibrational frequencies are in the range 60–100 cm<sup>-1</sup>. The second step at the HF level is also a, nucleophilic attack of CCl<sub>2</sub> on the  $\alpha$ -position of the pyrrole ring with the formation of

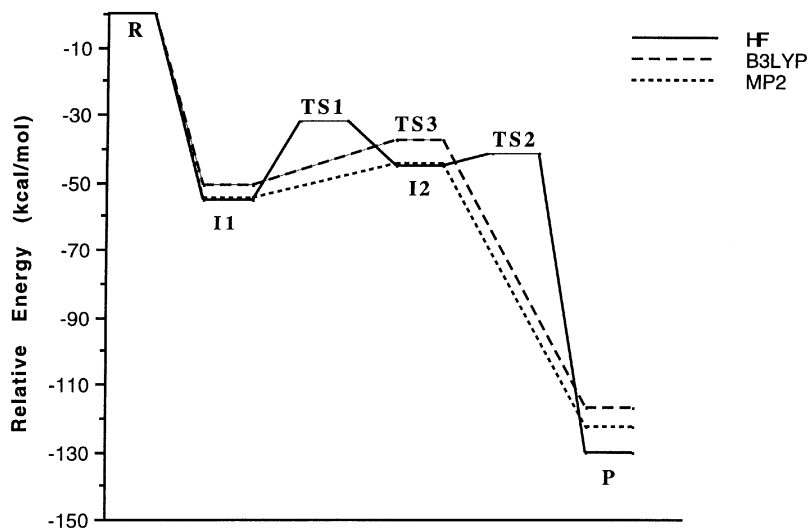


**Figure 1.** Schematic potential energy diagram showing the relative energies ( $\text{kcal mol}^{-1}$ ) of the stationary points located on the reactive potential energy surface *in vacuo*

the bicyclic intermediate **I2**, through transition structure **TS1**. The second step is associated with the cleavage of the C-2—C-3 bond of the pyrrole ring with concomitant ring expansion and a  $\text{Cl}^-$  leaving process, via **TS2**. However, B3LYP and MP2 calculations show a different energy profile; in both cases, only one transition structure **TS3**, is characterized on the reactive PES, associated with the cleavage of the C-2—C-3 and C-6—Cl-8 bonds and the formation of a C-6—C-2 bond via a synchronous mechanism.

The inclusion of the correlation energy promotes the flatness of the potential energy surface; the negative vibrational frequencies for **TS3** is around  $200\text{i cm}^{-1}$  whereas for **TS1** and **TS2**, obtained only at the HF level, the corresponding values are  $351\text{i}$  and  $556\text{i cm}^{-1}$ . The

force constants for those selected geometric parameters with non-zero components in the TV and the corresponding components of the control space for **TS1**, **TS2** and **TS3** are available from the authors on request. The C-6—C-2 distance is the main component of the TV for **TS1** whereas the C-2—C-3 and the C-6—Cl-8 bond distances make a large contribution to the corresponding TV for **TS2**. For **TS3**, three main components appear in TV: the C-2—C-3, C-6—C-2 and C-6—Cl-8 interatomic distances.

All computational methods describe the ring expansion process as an exothermic reaction, in the range from  $-117$  to  $-130 \text{ kcal mol}^{-1}$  ( $1 \text{ kcal} = 4.184 \text{ KJ}$ ), and the reaction pathway presents an inverted energy profile. The barrier height for the first activated chemical step at the

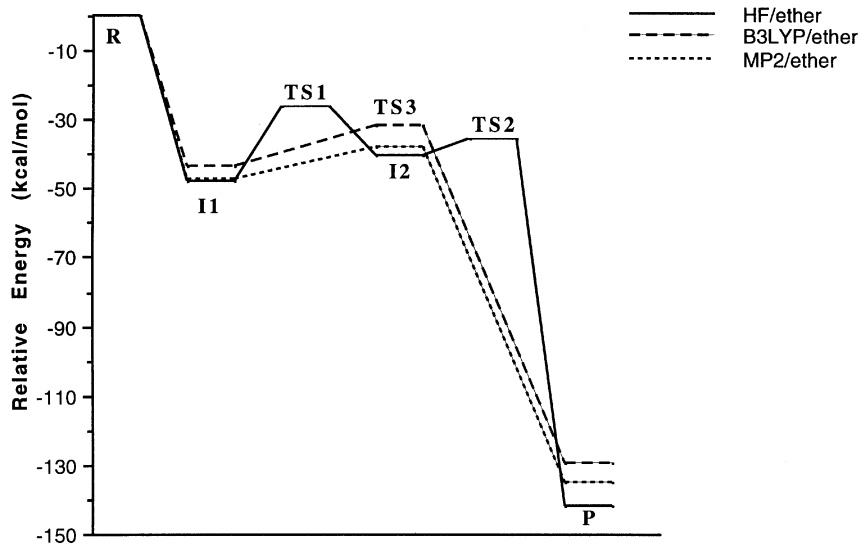


**Figure 2.** Schematic potential energy diagram showing the relative energies ( $\text{kcal mol}^{-1}$ ) of the stationary points located on the reactive potential energy surface in solvents

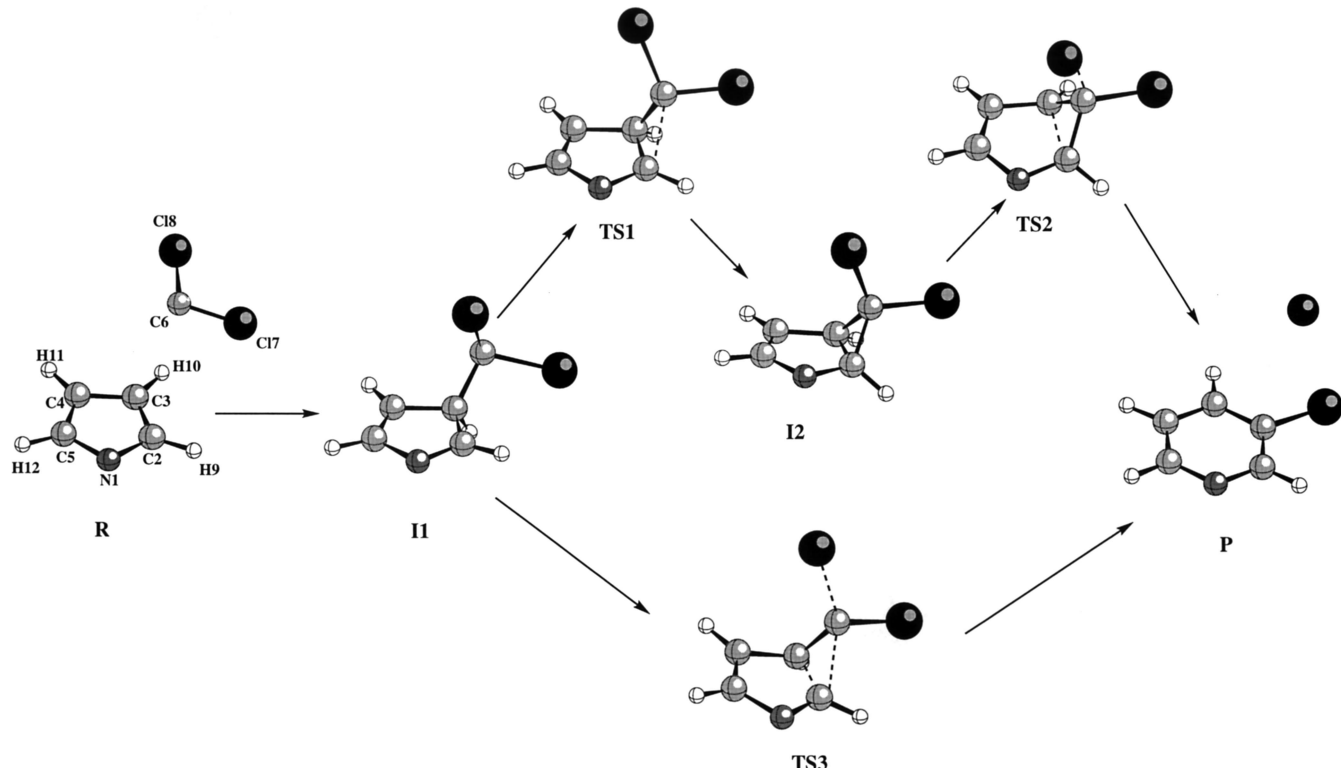


**Figure 3.** Representation of the stationary points for the abnormal Reimer–Tiemann reaction.

HF level,  $\mathbf{I}1 \rightarrow \mathbf{TS}1 \rightarrow \mathbf{I}2$ , is 23.7 kcal mol<sup>-1</sup> whereas the barrier height corresponding to the second step,  $\mathbf{I}2 \rightarrow \mathbf{TS}2 \rightarrow \mathbf{P}$ , is only 3.4 kcal mol<sup>-1</sup>. For the pathway described at the B3LYP and MP2 calculation levels, the barrier heights,  $\mathbf{I}1 \rightarrow \mathbf{TS}3 \rightarrow \mathbf{P}$ , are 13.2 and 10.6 kcal mol<sup>-1</sup> respectively. The inclusion of a diffuse function at the B3LYP/6-31+G\* level increases the relative energy of  $\mathbf{I}1$ ,  $\mathbf{TS}3$  and  $\mathbf{P}$ ; however, the geometries of stationary points and the main components of the TV do not change.

Our calculations have emphasized that the structures and energies of the stationary points are sensitive to the computational method. The qualitative features of the

reaction profile can be characterized in terms of two regions on the PES. There is a wide region corresponding to the initial step associated with the nucleophilic attack of the dichlorocarbene on the pyrrole ring system. The resulting surface is rather flat in this region. The details of the reaction path in the second region are very sensitive to the inclusion of electron correlation. As pointed out, at the HF/6-31G\* level, we have identified one intermediate,  $\mathbf{I}2$  defining a stepwise mechanism. Nevertheless, this shallow intermediate was only marginally stable and the presence of this stationary point is likely to be kinetically insignificant, i.e. the barriers for the conversion of  $\mathbf{I}2$  to  $\mathbf{P}$ , via  $\mathbf{TS}2$ , are low. The inclusion of electronic

**Table 1.** Relative energy (kcal mol<sup>-1</sup>) of the stationary points obtained *in vacuo* and in solvents, with the energy obtained with the diffuse function B3LYP/6-31+G\* (in parentheses)<sup>a</sup>

	HF	B3LYP (6-31+G*)	MP2	HF		B3LYP (6-31+G*)		MP2	
				Diethylether	Ethanol	Diethylether	Ethanol	Diethylether	Ethanol
<b>R</b>	0.00	0.00	(0.00)	0.00	0.00	0.00	(0.00)	0.00	0.00
<b>I1</b>	-55.54	-50.77	(-44.32)	-54.97	-47.68	-46.19	(-43.37)	(-35.21)	-42.15
<b>TS1</b>	-31.84	—	—	—	-26.32	-25.54	—	—	—
<b>I2</b>	-44.97	—	—	—	-40.17	-39.75	—	—	—
<b>TS2</b>	-41.53	—	—	—	-35.29	-34.02	—	—	—
<b>TS3</b>	—	-37.58	(-29.84)	-44.41	—	—	-31.51	(-20.76)	-30.38
<b>P</b>	-130.11	-116.65	(-112.60)	-122.47	-142.16	-144.35	-129.58	(-124.53)	-132.15

<sup>a</sup> Total energy of **R** = -1164.912435 au (HF), -1167.946051 au (B3LYP), -1167.985521 au (B3LYP/6-31+G\*), -1165.970341 au (MP2), -1164.988143 au (HF diethylether), -1165.009891 au (HF/ethanol), -1168.019576 au (B3LYP/diethylether), -1168.061080 au (B3LYP/6-31+G\*/diethylether), -1168.040384 au (B3LYP/ethanol), -1166.044689 au (MP2/diethylether), -1166.065859 (MP2/ethanol).

**Table 2.** Selected geometric parameters of the stationary points obtained with the different computing methods *in vacuo*, with the values obtained with the diffuse function B3LYP/6–31+G\* (in parentheses) (distances in ångstroms and bond and dihedral angles in degrees)

	<b>R</b>		MP2	<b>TS1</b>		MP2	HF
	HF	B3LYP (6–31+G*)		HF	B3LYP (6–31+G*)		
C-2-C-6	∞	∞ (∞)	∞	2.529	2.574 (2.568)	2.525	1.856
C-3-C-6	∞	∞ (∞)	∞	1.541	1.577 (1.565)	1.547	1.510
C-2-C-3	1.387	1.402 (1.407)	1.402	1.510	1.507 (1.508)	1.496	1.506
C-2-N-1	1.345	1.364 (1.365)	1.370	1.267	1.295 (1.296)	1.304	1.325
C-6-Cl-8	1.711	1.753 (1.747)	1.718	1.924	1.982 (1.956)	1.878	1.801
C-6-C-2-C-3	—	— (—)	—	112.00	113.18 (113.40)	112.10	52.14
H-9-C-2-N-1-C-5	180.00	180.00 (180.00)	180.00	180.74	179.41 (179.21)	178.68	189.17
	<b>I2</b>	<b>TS2</b>	B3LYP (6–31+G*)	<b>TS3</b>	<b>P</b>	B3LYP (6–31+G*)	MP2
	HF	HF		MP2	HF		
C-2-C-6	1.511	1.474	B3LYP (6–31+G*)	1.878 (1.896)	1.929	1.385	1.400 (1.398)
C-3-C-6	1.506	1.464		1.498 (1.500)	1.497	1.381	1.392 (1.393)
C-2-C-3	1.554	1.791	B3LYP (6–31+G*)	1.538 (1.534)	1.521	2.387	2.412 (2.414)
C-2-N-1	1.409	1.364		1.339 (1.340)	1.334	1.318	1.336 (1.337)
C-6-Cl-8	1.765	1.823	B3LYP (6–31+G*)	1.855 (1.852)	1.831	∞	∞ (∞)
C-6-C-2-C-3	58.85	52.20		50.82 (50.55)	49.74	30.25	30.09 (30.21)
H-9-C-2-N-1-C-5	210.27	205.44	B3LYP (6–31+G*)	187.60 (187.32)	184.98	180.00	180.00 (180.00)
							180.00

correlation energy modifies the energetic profile and only one transition structure, **TS3**, is located where the bond forming/breaking processes take place in a concerted manner.

### Solvent effect calculations

Because the inclusion of the solvent effects can be qualitatively and quantitatively significant,<sup>15,43</sup> the next step in our investigation was the study of the solvent effects on the basic features of the reaction pathway. The relative energies of the stationary points for both mechanisms in solution are given in Table 1 and the shapes of the corresponding reaction profiles *in vacuo* and in solution are depicted in Fig. 2. The relevant geometric data for the reactants, transition structures, intermediates and products in solution are presented in Table 3.

An analysis of the results shows that solute–solvent interactions lead to a slight change in the topology of the PES. The geometry of the stationary points located at the HF, MP2, B3LYP/6–31G\* and B3LYP/6–31+G\* levels are weakly dependent on solvent effects. The values of imaginary frequencies and the force constants of the components of the TV *in vacuo* and in a solvent are similar. The reaction pathway, as in the gas phase, presents an inverted energy profile and the exothermic character of the reaction is increased by more than 12 kcal mol<sup>-1</sup>. The solvent effects increase the relative energy of all stationary points with respect to **R**, except those for **P**. As could be expected from electrostatic arguments, the molecules with ionic character are stabilized when solvent effects are included. In addition,

an increment in the solvent polarity, on going from diethyl ether to ethanol, raises the aforementioned changes. The barrier height for the first step of the HF results decreases in the range 2.4–3.0 kcal mol<sup>-1</sup> while the second barrier height increases in the range 1.4–2.3 kcal mol<sup>-1</sup>. When electron correlation is included, the barrier height associated with **TS3** increases in the range 1.1–1.6 kcal mol<sup>-1</sup>.

A more balanced measure of the extent of bond formation or bond breaking along a reaction pathway is provided by the concept of bond order (*B*). This theoretical tool has been used to study the molecular mechanism of chemical reactions.<sup>44–46</sup> To follow the nature of the decomposition process, the Wiberg bond indices<sup>47</sup> were computed by using the natural bond orbital<sup>48,49</sup> analysis as implemented in Gaussian 94.

The progress of the chemical process at transition structure was then evaluated through the following expression:

$$\%_{\text{evolution}} = \frac{B(\text{TS}) - B(\text{X})}{B(\text{Y}) - B(\text{X})} \times 100 \quad (1)$$

where X and Y represent possible reactants/intermediates and intermediates/products, respectively, linked along a particular reaction pathway: X → TS → Y. Calculated percentages of evolution at the TSs *in vacuo* and in solvents are reported in Table 4.

An analysis of these data reveals a slight influence of the solvent effects on the percentage of bond breaking/forming processes at different transition structures. At the HF level, the percentage of the C-2–C-6 forming process at **TS1** decreases from 51.9% to 51.0% (diethylether) and to 50.4% (ethanol), while an opposite

**Table 3.** Selected geometric parameters of the stationary points obtained with the different computing methods in solvents, with the values obtained with the diffuse function B3LYP/6-31+G\* (in parentheses) (distances in ångstroms and bond and dihedral angles in degrees)

	R						I1			
	HF		B3LYP		MP2		HF		B3LYP	
	Diethylether	Ethanol	Diethylether	Ethanol	Diethylether	Ethanol	Diethylether	Ethanol	Diethylether	Ethanol
C—2—C—6	∞	∞	∞ (∞)	∞	∞	∞	2.546	2.544	2.563 (2.546)	2.571
C—3—C—6	∞	∞	∞ (∞)	∞	∞	∞	1.529	1.526	1.553 (1.558)	1.544
C—2—C—3	1.385	1.385	1.399 (1.405)	1.399	1.400	1.399	1.507	1.510	1.509 (1.508)	1.511
C—2—N—1	1.345	1.384	1.365 (1.367)	1.365	1.369	1.370	1.265	1.265	1.292 (1.292)	1.291
C—6—C18	1.708	1.707	1.748 (1.741)	1.745	1.714	1.713	1.910	1.979	1.974 (1.970)	1.950
C—6—C—2—C—3	—	—	— (—)	—	—	—	114.01	113.86	113.68 (112.22)	114.59
H—9—C—2—N—1—C—5	180.00	180.00	180.00 (180.00)	180.00	180.00	180.00	179.79	180.30	179.78 (179.41)	180.37
I1		TS1		I2		TS2		TS3		
MP2		HF		HF		HF		B3LYP		
Diethylether	Ethanol	Diethylether	Ethanol	Diethylether	Ethanol	Diethylether	Ethanol	Diethylether	Ethanol	
C—2—C—6	2.533	2.538	1.860	1.864	1.511	1.511	1.468	1.463	1.882 (1.898)	1.884
C—3—C—6	1.539	1.537	1.512	1.513	1.503	1.502	1.457	1.452	1.500 (1.502)	1.502
C—2—C—3	1.498	1.499	1.498	1.494	1.541	1.533	1.806	1.811	1.530 (1.530)	1.526
C—2—N—1	1.303	1.302	1.324	1.324	1.411	1.413	1.362	1.362	1.337 (1.340)	1.337
C—6—C1—8	1.895	1.896	1.806	1.811	1.767	1.769	1.845	1.864	1.879 (1.854)	1.889
C—6—C—2—C—3	113.00	113.45	52.17	52.16	59.00	59.11	51.59	51.34	50.92 (50.60)	50.97
H—9—C—2—N—1—C—5	179.64	180.32	190.38	191.03	211.91	212.96	206.48	207.17	188.71 (187.31)	189.33
TS3		P								
MP2		HF		B3LYP		MP2				
Diethylether	Ethanol	Diethylether	Ethanol	Diethylether	Ethanol	Diethylether	Ethanol			
C—2—C—6	1.926	1.927	1.381	1.380	1.392 (1.398)	1.392	1.396	1.396		
C—3—C—6	1.503	1.506	1.384	1.383	1.396 (1.393)	1.396	1.392	1.392		
C—2—C—3	1.514	1.510	2.389	2.389	2.413 (2.415)	2.413	2.414	2.415		
C—2—N—1	1.332	1.331	1.319	1.320	1.336 (1.338)	1.337	1.343	1.344		
C—6—C1—8	1.835	1.840	∞	∞	∞	∞	∞	∞		
C—6—C—2—C—3	50.07	50.20	30.17	30.14	30.02 (30.02)	29.98	29.96	29.92		
H—9—C—2—N—1—C—5	186.24	186.90	180.00	180.00	180.00 (180.00)	180.00	180.00	180.00		

**Table 4.** Percentages of evolution of the reaction at the **TS1**, **TS2** and **TS3** transition structures calculated through Eqn (2) for the C-2—C-3 and C-6—C-18 bond breaking processes and the C-2—C-6 bond forming process *in vacuo* and in solvents

		In Vacuo HF	Diethyl Ether HF	Ethanol HF
<b>TS1</b>	C—2—C—6	51.9	51.0	50.4
<b>TS2</b>	C—2—C—3	28.0	31.2	32.4
	C—6—C18	8.8	11.8	14.3
		B3LYP	MP2	B3LYP
<b>TS3</b>	C—2—C—3	9.2	4.8	7.9
3.9	7.2	3.5		
	C—2—C—6	33.8	24.2	33.6
24.1	33.3	23.8		
	C—6—C1—8	2.3	5.3	3.6
7.2	4.0	5.9		

trend is found at **TS2** for C-2—C-3 and C-6—Cl-8 bond breaking processes; from 28.0% to 31.2–32.4% (diethyl-ether, ethanol) and from 8.8% to 11.8–14.3% (diethyl-ether, ethanol), respectively. At the B3LYP and MP2 levels, the percentage of bond breaking/forming process increases slightly at **TS3**.

## CONCLUSIONS

We have carried out a theoretical study of the solvent effects along the reaction profiles on the corresponding PES for the abnormal Reimer–Tiemann rearrangement. The selected model is the reaction of the pyrrole system with dichlorocarbene to yield 3-chloropyridine. The reaction pathways were calculated using HF/6–31G\*, MP2/6–31G\*, B3LYP/6–31G\* and B3LYP/6–31+G\* methods in the gas phase and including solvent effects taking into account the polarizable continuum model. Our results show for the first time the nature of the molecular mechanism for the pyrrole ring expansion to yield 3-chloropyridine from theoretical calculations. The following conclusions can be drawn from the results:

(i) At the HF/6–31G\*, B3LYP/6–31G\*, B3LYP/6–31+G\* and MP2/6–31G\* levels, the first step corresponds to the nucleophilic attack of dichlorocarbene on C $\beta$  of the pyrrole ring with the formation of an intermediate in a barrierless fashion.

(ii) The theoretical results reveal that the general shape of the reaction profiles is sensitive to the inclusion of electron correlation. HF results show that two steps take place to obtain the final products. The first transition structure is associated with three-membered cyclization to form a new C-6—C-2 bond. Subsequent ring expansion, the C-2—C-3 cleavage process and leaving

of Cl $^-$  take place via the second transition structure. However, the inclusion of the correlation energy at the B3LYP and MP2 levels indicates that the molecular mechanism is a concerted process via the transition structure, **TS3**, and the C-2—C-3 and C-6—Cl-8 bond breaking and C-6—C-2 bond forming processes take place simultaneously.

(iii) For **TS3**, the cleavage of C-2—C-3, 7% is in a more advanced stage than that of C-6—Cl-8, 5%, while the C-6—C-2 bond forming process is around 30%.

(iv) The relative energies and barrier heights of the corresponding stationary points along the reaction pathways are invariant to the solvent effects and the inclusion of diffuse functions.

(v) The geometry of stationary points and the progress of the bond breaking/forming processes, the components of the transition vectors and the vibrational frequencies obtained in solution were essentially the same as those obtained in the gas phase.

## Acknowledgments

This work was supported by research funds of the Ministerio de Educación, DGICYT (Project PB93-0661). We are most indebted to the Servei d'Informàtica de la Universitat Jaume I for providing us with multiple computing facilities. M.O. thanks the Ministerio de Educación y Ciencia for an FPI fellowship and R.C. thanks Silicon Graphics for a fellowship.

## REFERENCES

1. G. L. Fritz, G. D. Mills and J. D. Warthen. *J. Chem. Ecol.* **15**, 2607 (1989).
2. J. C. Cochran and M. G. Melville. *Synth. Commun.* **20**, 609 (1990).
3. B. R. Langlois. *Tetrahedron Lett.* **32**, 3691 (1991).
4. A. V. Gaonkar. *Indian J. Chem. Sect. B* **30**, 800 (1991).
5. S. Divakar, M. M. Maheswaran and M. S. Narayan. *Indian J. Chem., Sect. B* **31**, 543 (1992).
6. M. C. Jimenez, M. A. Miranda and R. Tormos. *Tetrahedron* **51**, 5825 (1995).
7. M. E. Jung and T. I. Lazarova. *J. Org. Chem.* **62**, 1553 (1997).
8. E. R. Alexander, A. B. Herrick and T. M. Roder. *J. Am. Chem. Soc.* **72**, 2760 (1950).
9. H. Wynberg. *J. Am. Chem. Soc.* **76**, 4998 (1954).
10. J. Hine and J. M. van der Veen. *J. Am. Chem. Soc.* **81**, 6446 (1959).
11. H. Wynberg. *Chem. Rev.* **60**, 169 (1960).
12. D. S. Kemp. *J. Org. Chem.* **36**, 202 (1970).
13. H. Wynberg and E. W. Meijer. *Organic Reactions*, Vol. 28, Wiley, New York (1982).
14. J. Andrés, J. J. Queralt, V. S. Safont, L. M. Canle and J. A. Santabarria. *J. Phys. Chem.* **100**, 3561 (1996).
15. L. R. Domingo, M. T. Picher, J. Andrés, V. Moliner and V. S. Safont. *Tetrahedron* **52**, 10693 (1996).
16. V. Moliner, R. Castillo, V. S. Safont, M. Oliva, S. Bohm, I. Tuñón and J. Andrés. *J. Am. Chem. Soc.* **119**, 1941 (1997).
17. M. J. Frisch, G. W. Trucks, H. B. Schlegel, P. M. W. Gill, B. G. Johnson, M. A. Robb, J. R. Cheeseman, T. Keith, G. A. Petersson, J. A. Montgomery, K. Raghavachari, M. A. Al-Laham, V. G. Zakrzewski, J. V. Ortiz, J. B. Foresman, J. Ciosowski, B. B. Stefanov, A. Nanayakkara, M. Challacombe, C. Y. Peng, P. Y. Ayala, W. Chen, M. W. Wong, J. L. Andres, E. S. Replogle, R.

- Gomperts, R. L. Martin, D. J. Fox, J. S. Binkley, D. J. Defrees, J. Baker, J. P. Stewart, M. Head-Gordon, C. Gonzalez and J. A. Pople. *Gaussian 94*. Gaussian, Pittsburgh, PA (1995).
18. C. Moller and M. S. Plesset. *Phys. Rev.* **46**, 618 (1934).
19. J. Andzelm and E. Wimmer. *J. Chem. Phys.* **96**, 1280 (1992).
20. F. Sim, A. St-Amant, I. Papai and D. R. Salahub. *J. Am. Chem. Soc.* **114**, 4391 (1991).
21. P. M. W. Gill, B. G. Johnson, J. A. Pople and M. Frisch. *Chem. Phys. Lett.* **197**, 499 (1992).
22. A. D. Becke. *Phys. Rev. A* **38**, 3098 (1988).
23. A. D. Becke. *J. Chem. Phys.* **98**, 5648 (1993).
24. C. Lee, W. Yang and R. G. Parr. *Phys. Rev. B* **37**, 785 (1988).
25. B. Miehlich, A. Savin, H. Stoll and H. Preuss. *Chem. Phys. Lett.* **157**, 200 (1989).
26. O. Tapia and J. Andres. *Chem. Phys. Lett.* **109**, 471 (1984).
27. J. Andrés, V. Moliner and V. S. Safont. *J. Chem. Soc., Faraday Trans.* **90**, 1703 (1994).
28. O. Tapia, J. Andrés and V. S. Safont. *J. Chem. Soc., Faraday Trans.* **90**, 2365 (1994).
29. J. Baker. *J. Comput. Chem.* **7**, 385 (1986).
30. J. Baker. *J. Comput. Chem.* **8**, 563 (1987).
31. K. Fukui. *J. Phys. Chem.* **74**, 4161 (1970).
32. C. González and H. B. Schlegel. *J. Phys. Chem.* **94**, 5523 (1990).
33. C. González and H. B. Schlegel. *J. Chem. Phys.* **95**, 5853 (1991).
34. H. B. Schlegel. *J. Comput. Chem.* **3**, 214 (1982).
35. H. B. Schlegel. *J. Chem. Phys.* **77**, 3676 (1982).
36. J. W. J. McIver. *Acc. Chem. Res.* **7**, 72 (1974).
37. R. Rinaldi and R. R. S. Pappalardo. *QCPE*. Indiana University, Bloomington, IN (1992).
38. T. Tomasi and M. Persico. *Chem. Rev.* **94**, 2027 (1994).
39. J. L. Rivail and D. Rinaldi. *Chem. Phys.* **18**, 233 (1976).
40. J. L. Rivail, D. Terryn, D. Rinaldi and M. F. Ruiz-López. *J. Mol. Struct. (THEOCHEM)* **120**, 387 (1985).
41. D. Rinaldi, J. L. Rivail and N. J. Rguini. *J. Comput. Chem.* **13**, 675 (1992).
42. V. Dillet, D. Rinaldi, J. G. Angyan and J. L. Rivail. *Chem. Phys. Lett.* **202**, 18 (1993).
43. J. Andrés, S. Bohm, V. Moliner, E. Silla and I. Tuñón. *J. Phys. Chem.* **98**, 6955 (1994).
44. A. J. C. Varandas and S. J. F. Formosinho. *J. Chem. Soc., Faraday Trans. 2* **82** (1986).
45. G. Lendvay. *J. Mol. Struct. (THEOCHEM)* **167**, 331 (1988).
46. G. Lendvay. *J. Phys. Chem.* **93**, 4422 (1989).
47. K. B. Wiberg. *Tetrahedron* **24**, 1083 (1968).
48. A. E. Reed, R. B. Weinstock and F. J. Weinhold. *J. Chem. Phys.* **83**, 735 (1985).
49. A. E. Reed, L. A. Curtiss and F. Weinhold. *Chem. Rev.* **88**, 899 (1988).